Shear-Flexure Interaction for Structural Walls

by L.M. Massone, K. Orakcal, and J.W. Wallace

Synopsis: An analytical model that couples the flexural and shear responses of reinforced concrete structural walls is proposed. The proposed modeling approach involves incorporating RC panel behavior into a macroscopic fiber-based model. Results obtained with the analytical model are compared with test results for a slender wall and four short wall specimens. A reasonably good lateral load-displacement response prediction is obtained for the slender wall. The model underestimates the inelastic shear deformations experienced by the wall; however, shear yielding and coupled nonlinear shear-flexure behavior are successfully represented in the analysis results. The model captures accurately the measured responses of selected short walls with relatively large shear span ratios (e.g., 1.0 and 0.69). Discrepancies are observed between the analytical and experimental results as wall shear span ratios decrease (e.g., 0.56 and 0.35). Better response predictions can be obtained for walls with low shear span ratios upon improving the model assumptions related to the distribution of stresses and strains in a wall.

Keywords: fiber; flexure; interaction; model; panel; reinforced concrete; shear; wall

Leonardo Massone is a PhD student in the Department of Civil Engineering, UCLA, and an Instructor Professor on leave from the University of Chile. He received his B.S. from the University of Chile in 1999, and his M.S. in Civil Engineering from UCLA in 2003. His research interests include analytical and experimental studies of reinforced concrete elements and systems.

Kutay Orakcal is a Post-Graduate Researcher in the Department of Civil Engineering, UCLA. He received his BS from Middle East Technical University in 1998, his MS from UCLA in 2001, and his PhD in civil engineering from UCLA in 2004. His research interests include behavior and modeling of reinforced concrete elements and systems.

John W. Wallace, FACI, is an professor of civil engineering at UCLA, Los Angeles, California. He is a voting member of ACI Committees 318-H, 374, and Joint ACI-ASCE Committee 352. His research interests include response and design of buildings and bridges to earthquake actions, laboratory and field testing of structural components and systems, and structural health monitoring and use of sensor networks.

INTRODUCTION

Reinforced concrete (RC) structural walls are commonly used to resist the actions imposed on buildings due to earthquake ground motions. To resist such actions, properly proportioned and detailed slender walls are designed to yield in flexure, and to undergo inelastic flexural deformations without loss of lateral load capacity. Therefore, the ability to model the cyclic behavior and failure modes of structural walls is an important aspect of engineering design, particularly as the profession moves forward with design and evaluation approaches that emphasize performance based seismic design.

Recent research has shown that the lateral force versus deformation response of slender walls in flexure can be captured reasonably well using simple analytical models (e.g., Thomsen and Wallace, 2004), and improved predictions can be obtained using more detailed models (e.g., Orakcal et al., 2004). However, such models usually consider uncoupled shear and flexural responses, which is inconsistent with experimental observations, even for relatively slender walls (Massone and Wallace, 2004).

Analytical models have been proposed to consider the observed coupling between flexural and shear components of RC wall response. A recognized methodology involves implementing the finite element method together with a constitutive RC membrane model that follows a rotating-angle modeling approach (e.g., Modified Compression Field Theory, Vecchio and Collins, 1986; Rotating Angle Softened Truss Model, Pang and Hsu, 1995). A methodology based on adopting this idea for a fiber model, was proposed by Petrangeli et al. (1999) to couple shear response with flexural and axial responses.

The analytical model proposed in this study is based on applying the methodology developed by Petrangeli to a macroscopic fiber-based model (Multiple-Vertical-Line-Element-Model, Vulcano et al., 1988). A description of the proposed modeling approach

to incorporate coupling of wall flexural and shear responses is presented. Preliminary model results are compared with test results obtained from tests on a slender wall and four short wall specimens to evaluate the modeling approach. The accuracy and limitations of the model are emphasized to identify model capabilities as well as ways to improve the model.

DESCRIPTION OF THE ANALYTICAL MODEL

Base model: Multiple-Vertical-Line-Element Model (MVLEM)

The Multiple Vertical Line Element Model (MVLEM) resembles a two-dimensional fiber model, simplified such that element rotations (curvatures) are concentrated at the center of rotation defined for each element. In the MVLEM, a single average value of curvature is assumed for each model element, as opposed to a generic displacement-based fiber model implementation where a linear curvature distribution (displacement interpolation function) is used between element nodes and the curvature distribution is integrated at Gauss points to obtain element rotations and displacements. A structural wall is modeled as a stack of MVLE's, which are placed one upon the other, and the coupled axial-flexural response of each MVLE is simulated by a series of uniaxial elements (or macro-fibers) connected to infinitely rigid beams at the top and bottom (e.g., floor) levels (Fig. 1(a)), that enforce a plane section assumption. A horizontal spring placed at the center of rotation (at relative height *ch*) of each MVLE, with a prescribed nonlinear force-deformation behavior, is commonly used to simulate the shear response of the element. Shear and flexural responses are considered uncoupled in the original formulation of the MVLEM. The constitution and kinematics of the MVLEM are explained in detail in Orakcal et al. (2004).

Displacement interpolation functions

The original formulation of the Multiple-Vertical-Line-Element Model is modified in this study to accommodate displacement interpolation functions and integration (Gauss) points for practical implementation of the model into computational platforms (e.g., OpenSees), in which the displacement-based fiber model formulation is already built in. However, derivation of the displacement interpolation functions implemented in the model incorporate the definition of an element center of rotation in order to distinguish between model lateral displacements resulting from shear and flexural deformations. The element center of rotation is defined at a fraction of the element height *ch*, as in the case of the original MVLEM.

In an attempt to locate the center of rotation in a slender cantilever wall, experimental results from Sayre (2003) were investigated by Massone and Wallace (2004). Curvature distributions measured by linear transducer (LVDT) pairs were used to evaluate the center of rotation along the first story level of a slender steel reinforced concrete wall specimen. Experimental data points were found to give an average center of rotation coefficient of $c = 0.4$ for the entire loading range, without significant scatter of the data when the wall is subjected to nonlinear deformations. Therefore, a value of $c = 0.4$ is used in this study. Use of $c = 0.4$ is also consistent with the studies by Vulcano et al.

(1988) and Orakcal et al. (2004), who recommended the same value for c, based on comparison of the analysis results using the MVLEM with results of wall tests.

The displacement interpolation functions implemented into the analytical model represent the three displacement field components shown in Fig. 1, which are associated with the axial (u), flexural (w_f) and shear (γ) deformations of the element. Other than implementing the idea of a center of rotation to segregate model transverse displacements into shear deformation (integration of shear strain) and flexural deformation (integration of curvature distribution) components, the derivation of the displacement interpolation functions considers a linear variation of axial deformations and curvatures, and a uniform distribution of shear strain along the longitudinal axis (y) of the model element. Accordingly, the displacement field of the 2-node model element, with respect to the 6 degrees of freedoms illustrated in Fig. 1(a) is obtained as:

$$\begin{bmatrix} u(y) \\ w_f(y) \\ \gamma(y) \end{bmatrix} = \begin{bmatrix} 1-y/h & 0 & 0 & y/h & 0 & 0 \\ 0 & 1 & yc_1 & 0 & 0 & -yc_1+y \\ 0 & -1/h & -c & 0 & 1/h & c-1 \end{bmatrix} \cdot \begin{bmatrix} u_0 \\ w_0 \\ \theta_0 \\ u_h \\ w_h \\ \theta_h \end{bmatrix} = \underline{N}(y) \cdot U_N \quad (1)$$

where $c_1 = 1 + (3c-2)y/h + (1-2c)(y/h)^2$ (2)

and where $N(y)$ represents the element displacement interpolation functions for axial, flexural and shear deformations, and U_N is the set of element nodal displacements.

Modeling of shear-flexure interaction

The analytical model proposed in this study incorporates RC panel behavior in the Multiple-Vertical-Line-Element-Model (the original formulation of which considers uncoupled flexural and shear responses), in order to capture the experimentally observed shear-flexure interaction in RC walls (e.g., Massone and Wallace, 2004). The proposed wall model involves modifying the MVLEM by assigning a shear spring for each uniaxial element. Each uniaxial element is then treated as a RC panel element, with membrane actions, i.e., uniform normal and shear stresses applied in the in-plane direction. Therefore, the interaction between flexure and shear is incorporated at the uniaxial element (fiber) level. To represent constitutive panel behavior, a rotating-angle modeling approach, as applied in the derivation of the Modified Compression Field Theory (MCFT, Vecchio and Collins, 1986) or the Rotating-Angle Softened-Truss-Model (RA-STM, Pang and Hsu, 1995), can be used. The constitutive rotating-angle modeling approach adopted in this study follows the RA-STM; however, a more refined constitutive stress-strain model for concrete in compression, which is calibrated with a large set of experimental results, is implemented. Constitutive stress-strain models for materials are applied along the principal directions of the strain field (i.e., principal strain directions 1 and 2), to obtain the stress field associated with the principal directions. It is assumed that the principal stress and strain directions coincide (as suggested by Vecchio and Collins, 1986; Pang and Hsu, 1995).

Accordingly, the axial and shear responses of each uniaxial (panel) element are coupled, which further allows coupling of flexural and shear responses of the MVLEM, since the axial response of the uniaxial elements constitute the overall flexural response of each MVLE. Details of the methodology are described in the following subsection.

Numerical methodology for the proposed model

In the description of the methodology, the uniaxial (panel) elements located within each model element (also called strips) are denoted by (i) and the model elements are denoted by (j):

1. The deformations or strains within the components of each element (j) are determined from the six prescribed degrees of freedom, (u_x, u_y and θ at both ends of the model element) shown in Fig. 2. Assuming that the shear strain is uniform along the section and that plane sections remain plane, the axial strain (ε_y) and shear distortion (γ_{xy}) components of the strain field are calculated for the entire section (for all the strips (i)) based on the prescribed degrees of freedom for the current analysis step. Accordingly, each strip (i) (Fig. 2) has two input variables, axial strain (ε_y) and shear distortion (γ_{xy}), based on element (j) deformations. The horizontal (or transverse) normal strain within each strip (ε_x) is initially estimated to complete the definition of the strain field, allowing stresses and forces to be determined from the constitutive material relationships and geometric properties (dimensions and reinforcement and concrete areas) for each strip. For the initial estimate of the horizontal strain within each strip (ε_x), a zero value or the resulting value from the previous load step can be used. The output variables associated with the input strains ε_y and γ_{xy} are the axial stress, σ_y, and the shear stress, τ_{xy}, for each strip (i).

2. A numerical procedure (Newton's method) is employed to linearize the equilibrium equation and iterate on the unknown quantity ε_x (horizontal normal strain in each strip i), to achieve horizontal equilibrium for a given σ_x (resultant horizontal normal stress) within each strip. The horizontal stress σ_x is the resultant of stress components in concrete and steel which balances normal stress resulting from loads applied in the horizontal direction. Due to a lack of information and as an initial approximation, the horizontal stress σ_x within each strip was assumed to be equal to zero (no resultant stress), which is consistent with the boundary conditions at the sides of a wall with no transverse loads applied over its height. The orientation of principal strain (or stress), α, is used as an iterative parameter (instead of ε_x) for convenience.
    a) For a trial value of principal orientation angle (α, together with the prescribed values of axial strain (ε_y) and shear distortion (γ_{xy})), the strain field (horizontal strain ε_x, and the principal strains ε_1 and ε_2) is defined for each strip (i). It is assumed that the same orientation angle (α) applies for the principal directions of both the strain (ε_1, ε_2) and the stress fields (σ_{c1}, σ_{c2}). Using the constitutive material relationships implemented for concrete and steel, and compatible strains for the two materials (assuming perfect bond), the stresses in concrete along the principal directions and stresses in reinforcement along the vertical and horizontal directions are determined. As noted earlier, a uniaxial stress-

strain model is used for the reinforcing steel; therefore, stresses in reinforcement are calculated in horizontal and vertical directions (based on ε_x and ε_y, based on the assumption that reinforcement is provided in the vertical and horizontal directions, or transformed to equivalent reinforcement in the horizontal and vertical directions).

b) Stresses in concrete are transformed from the principal directions to the reference coordinate directions (x-y) and the resulting concrete forces are superimposed with the forces in the reinforcement based on the concrete and steel areas within each strip. The resultant gives average normal and shear stresses in each strip (i) as:

$$\tau_{xy} = -\frac{\sigma_{c1} - \sigma_{c2}}{2} \cdot \sin(2 \cdot \alpha) \tag{3}$$

$$\sigma_x = \sigma_{cx} + \rho_x \cdot \sigma_{sx} = \frac{\sigma_{c1} + \sigma_{c2}}{2} - \frac{\sigma_{c1} - \sigma_{c2}}{2} \cdot \cos(2 \cdot \alpha) + \rho_x \cdot \sigma_{sx} \tag{4}$$

$$\sigma_y = \sigma_{cy} + \rho_y \cdot \sigma_{sy} = \frac{(\sigma_{c1} + \sigma_{c2})}{2} + \frac{(\sigma_{c1} - \sigma_{c2})}{2} \cdot \cos(2 \cdot \alpha) + \rho_y \cdot \sigma_{sy} \tag{5}$$

c) Equilibrium is checked in the horizontal direction (σ_x) for each strip (i), until equilibrium is achieved for the specified angle α

3. Once horizontal equilibrium is achieved for a specified tolerance within each strip, vertical stresses in the strips are assembled to determine the total resisting axial force and bending moment of each element, whereas the shear forces in the strips are assembled to determine the total resisting shear force of the element.

4. Consequently, global equilibrium is checked for the overall wall model by comparing the applied and resisting forces, and global iterations are performed on the model degrees of freedom until global equilibrium is satisfied.

MATERIAL CONSTITUTIVE MODELS

As described in the previous section, the proposed modeling approach involves using two dimensional RC panel elements subjected to membrane actions, where the stiffness and force-deformation properties of the panel elements are derived directly from material stress-strain relations. Therefore, details of the constitutive relationships used in this study for reinforcing steel and concrete are described in this section.

Constitutive model for reinforcing steel

The stress-strain relationship implemented in the wall model for reinforcing steel is the well-known uniaxial constitutive model of Menegotto and Pinto (1973). The relationship is in the form of curved transitions (Fig. 3), each from a straight-line asymptote with slope E_0 (modulus of elasticity) to another asymptote with slope $E_1=bE_0$ where parameter b is the strain hardening ratio. The curvature of the transition curve between the two asymptotes is governed by the parameter R (Fig. 3), the cyclic degradation of which permits the Bauschinger effect to be represented. Cyclic properties of constitutive relationship are not incorporated in the present wall model; the model is yet to be

extended for cyclic analysis. However, the cyclic stress-strain response generated by the model is also illustrated in Fig. 3 for further discussions.

To consider the effects of tension stiffening on reinforcement, Belarbi and Hsu (1994) developed alternative average tensile stress-strain relationships for steel bars embedded in concrete. The so-called single-curve model can be directly incorporated in the Menegotto and Pinto equation, and has been used for the calibration of the present wall model. As proposed by Belarbi and Hsu, the effective yield stress and strain (intersection of the elastic and yield asymptotes) for bars embedded in concrete correspond to approximately 91% of the yield stresses and strains of bare bars and the monotonic curvature parameter R_0 is described by the following empirical relation:

$$R_0 = \frac{1}{9B - 0.2} \leq 25 \qquad \text{where} \qquad B = \frac{1}{\rho}\left(\frac{f_{cr}}{\sigma_y}\right)^{1.5} \tag{6}$$

where f_{cr} is the concrete cracking stress and ρ is the cross-sectional area ratio of the longitudinal steel bars in the RC element (limited to a minimum of 0.25% in Mansour et al., 2001). The monotonic curvature parameter R_0 is limited to a value of 25, where the limiting value practically represents a sharp corner between the elastic and yield asymptotes.

The so called "kinking effect" (reduction of effective yield stress due to dowel action along the cracks) incorporated by Pang and Hsu (1995) in the original Rotating-Angle Softened-Truss-Model is disregarded in this study based on later experimental observations by Hsu and Zhu (2002), who stated that the kinking effect can be neglected.

Constitutive model for concrete

To obtain a reliable model for panel (membrane) behavior, the constitutive relationship implemented in the analytical model for concrete should consider the effects of biaxial compression softening (reduction in principal compressive stresses in concrete due to cracking under tensile strains in the orthogonal direction), and tension stiffening (average post-peak tensile stresses in concrete due to the bonding of concrete and reinforcing steel between cracks). Properties of the constitutive model adopted in this study for concrete are described in this subsection.

To incorporate the tension stiffening effect in the stress-strain behavior of concrete in tension, the average (smeared) stress-strain relationship proposed by Belarbi and Hsu (1994) (Fig. 4) is implemented. To describe the stress-strain behavior of concrete in compression, the Thorenfeldt base curve, calibrated by Collins and Porasz (1989), Wee et al. (1996) and Carreira and Kuang-Han (1985), and updated via the introduction of the compression softening parameter proposed by Vecchio and Collins (1993), is used. The Thorenfeldt base curve, which is based on the Popovics (1973) equation, takes the form (Fig. 5):

$$\sigma_c = f_c^{'} \frac{n\left(\frac{\varepsilon_c}{\varepsilon_0}\right)}{n-1+\left(\frac{\varepsilon_c}{\varepsilon_0}\right)^{nk}} \tag{7}$$

where $f_c^{'}$ is the peak compressive stress (e.g., concrete compressive cylinder strength) and ε_0 is the strain at peak compressive stress for unconfined concrete in compression. For defining of the strain at peak compressive stress (ε_0), the expression proposed by Wee et al. (1996) is used (Fig. 5). The following expressions proposed by Collins and Porasz (1989) are used for the equation parameters n and k, for calibration of the model for relatively high-strength concrete:

$$n = 0.8 + \frac{f_c^{'}(MPa)}{17} \tag{8}$$

and $k = 1$ when $0 \le \varepsilon \le \varepsilon_0$ (9)

$$k = 0.67 + \frac{f_c^{'}(MPa)}{62} \quad \text{when} \quad \varepsilon_0 \le \varepsilon \tag{10}$$

For concrete with lower compressive strengths (e.g., $f_c^{'} < 20$ MPa), the following expressions proposed by Carreira and Kuang-Han (1985) are considered for the same parameters:

$$n = 1.55 + \left(\frac{f_c^{'}(MPa)}{32.4}\right)^3 \tag{11}$$

$$k = 1 \tag{12}$$

An important consideration in modeling the behavior of a RC panel element under membrane actions is incorporating the compression softening effect. Vecchio and Collins (1993) used a large experimental database from tests on RC panels to propose different models representing compression softening. The so-called Model B, which considers a reduction in peak compressive stress, is implemented in this study since Vecchio and Collins (1993) observed that more complicated models are only marginally better for incorporating the compression softening effect. Accordingly, the reduction factor to be applied to the peak compressive stress for concrete in compression (Fig. 5) is given by the expression:

$$\beta = \frac{1}{0.9 + 0.27\frac{\varepsilon_1}{\varepsilon_0}} \tag{13}$$

where ε_1 is the principal tensile strain, and the ratio $\varepsilon_1/\varepsilon_0$ is considered positive.

COMPARISON OF MODEL RESULTS WITH EXPERIMENTS

The proposed analytical model integrates the material models described in the previous section with a rotating-angle modeling approach to assemble a constitutive RC panel

model. In modeling of the wall response, the analytical model, as implemented in this study, incorporates further assumptions including the plane sections remain plane kinematic assumption, a uniform distribution of shear strains along wall length, and an assumed zero value for the resultant horizontal stress (σ_x) within each strip of the model element. Due to the simplifications associated with the implemented material models, idealizations of the rotating-angle modeling approach (e.g., principal strain and stress fields coincide assumption), and the assumptions involved in the formulation of the present wall model (plane sections, uniform shear strains, zero horizontal stresses), the validity of the model needs to be investigated for different wall configurations. Therefore, this section presents information on correlation of preliminary model results with experimental results in order to evaluate the modeling approach. First, results of the constitutive panel model are compared to experimental results from RC panel tests to validate the response of model sub-elements. Then, the responses simulated by the wall model are compared to test results on slender and short wall specimens. A discussion based on experimental observations, regarding a specific model assumption (i.e., uniform shear strain distribution along wall length), is also provided.

Panel behavior

To verify the constitutive material models selected and the constitutive panel behavior incorporated in the present wall model, results from tests conducted by prior researchers on RC panel specimens subjected to pure shear loading conditions are compared to analytical responses obtained using the constitutive panel model adopted. Two different test series are used here for the comparisons (series A&B and series PV). Series A and B were tested by Pang and Hsu (1995). The RC panel specimens tested were 1.4 m x 1.4 m x 178 mm thick, and were uniformly reinforced with reinforcement area ratios varying between 0.6% and 3%. In-plane loads were applied such that an equivalent pure shear loading condition (orthogonal to the reinforcement) was achieved. Series PV specimens were tested by Vecchio and Collins (1982). The specimens had dimensions of 0.89 m x 0.89 m x 70 mm thick, and were uniformly reinforced with reinforcing ratios varying between 0.7 and 1.8%. Pure shear loads were applied along the sides of the specimens.

The constitutive panel element used in the present study was calibrated based on the material properties and specimen geometry of selected test specimens, and subjected to a pure shear loading condition to simulate the test conditions. Accordingly, comparisons of analytical results with experimental results for the shear stress – shear strain response of the selected panels are shown in Fig 6. As observed in the Fig. 6, good correlation is obtained between the element responses and test results, validating the selection of the constitutive material models and the formulation of the panel elements incorporated in the present wall model. However, it must be noted that the correlations presented are not for generalized loading conditions; responses under only pure shear loading conditions are considered.

Slender wall response

Experimental observations indicate coupling between shear and flexural responses, even for relatively slender walls (e.g., Massone and Wallace, 2004). Thus, correlation of preliminary model results with results from a slender wall test is presented.

Test overview – The rectangular wall specimen (specimen RW2) tested by Thomsen and Wallace (2004) was proportioned using a capacity design approach and boundary element details were based on using a displacement-based design methodology. Sufficient shear capacity was provided for the wall specimen to resist the shear that developed for the probable wall moment, using ACI 318-89 (1989) (Eq. 21-6). The wall specimen was 3.66 m tall and 102 mm thick, with a web length of 1.22 m. Design concrete compressive strength (f_c') was 27.5 MPa, and Grade 60 (f_y=414 MPa) bars were used for longitudinal and web reinforcement of the specimen. The wall specimen was tested in an upright position, and an axial load of approximately $0.07A_g f_c'$ was held constant throughout the duration of the test. Cyclic lateral displacements were applied at the top of the wall using a hydraulic actuator. Instrumentation was used to measure displacements, loads, and strains at critical locations for the wall specimen. Wire potentiometers were mounted to a rigid steel reference frame to measure wall lateral displacements along wall height. Shear deformations were measured through the use of wire potentiometers mounted on the bottom two stories (in an "X" configuration) of the wall. To calculate wall rotations, axial (vertical) displacements at the wall boundaries were measured using two wire potentiometers mounted directly to the wall boundaries. More detailed information concerning the wall tests is presented in Thomsen and Wallace (2004).

Model calibration – To discretize the wall cross section for the analytical model, 16 strips (panel elements) were defined along the length of the wall specimen, with corresponding tributary areas for concrete and vertical reinforcement assigned to each strip. The horizontal reinforcement area was set constant for all of the strips, which was consistent with the horizontal reinforcement used for the specimen. A total of 8 model elements (each consisting of 16 strips) were stacked along the height of the wall. A more refined discretization of the wall (with a larger number of strips and model elements) did not change considerably the model response obtained for the wall specimen. The constitutive relationships implemented in the model for reinforcing steel and concrete were calibrated to represent the experimentally observed properties of the materials used in the experimental study (using results of monotonic stress-strain tests conducted on concrete and rebar specimens). Confinement and tension stiffening effects were incorporated as discussed by Orakcal and Wallace (2004).

Model correlation with test results – Prior to analysis, the experimental results for wall lateral displacements at story levels were separated into flexural and shear response components using the methodologies described by Massone and Wallace (2004) to allow comparison of model results to local (e.g., story) shear and flexural response measurements. Results of monotonic analysis with the proposed model were compared with the cyclic test results for the slender wall specimen.

Figure 7 compares the analytical and experimental lateral load – top displacement responses for the wall specimen. As observed in Fig. 7, the lateral load capacity and the lateral stiffness of the wall are significantly overestimated for lower lateral drift levels (i.e., up to 0.75% drift), and overestimated to a lesser extent for higher lateral drift levels. The overestimation of the wall capacity and stiffness, especially at lower drifts can be attributed to the fact that analysis results for monotonic loading are compared to cyclic test results. Cyclic degradation of the curvature parameter R (Fig. 3) associated with the implemented constitutive model for reinforcing steel, influences significantly the wall lateral load capacity and stiffness prediction, especially within the pre-yield and relatively low post-yield drift levels (Orakcal et al., 2004). The present monotonic constitutive model for reinforcement does not consider the cyclic degradation of the parameter R, impairing the response prediction. It must be noted that results presented are preliminary, and additional studies to incorporate cyclic behavior and to improve the material relations for a more refined calibration are underway.

Figure 8 presents the correlation of analytical and experimental results for the lateral load – flexural displacement and lateral load – shear displacement responses at the first story level of Specimen RW2. The figure reveals that the model overestimates the flexural deformations and underestimates the shear deformations measured within the first story of the wall specimen. Again, the correlations would be significantly improved upon incorporating cyclic analysis. However, as observed in the figures, the model is capable of capturing the nonlinear shear deformations experienced simultaneously with the nonlinear flexural deformations within the first story of the wall specimen, and thus successfully incorporates coupling of nonlinear shear and flexural responses that were observed experimentally, even for this relatively slender wall.

Short wall response

As mentioned earlier, the proposed methodology to couple shear and flexural responses involves three main assumptions: shear strains are uniformly distributed across the wall cross section, the resultant horizontal stresses along the length of the wall are zero, and plane sections remain plane. In the case of tall walls, the first assumption (i.e., uniform distribution of shear strain) may not influence significantly the overall wall response since the governing response component is flexure. However, for short walls, using the same assumption may not be reasonable due to possible presence of different modes of deformation (e.g., warping) or different load transfer mechanisms (e.g., strut action), or other possible reasons such as the so called Saint-Venant's effect, where the relatively small height of the wall may not be adequate to allow redistribution of stresses concentrated within the proximity of the points of load application or where support reactions are present. Such effects introduce non-uniformity in stresses and strains that may change considerably the observed wall response. A similar condition applies to the zero horizontal stress and plane section assumptions.

Thus, correlation of model results with test results on short wall specimens is presented to assess the validity of the modeling approach for short walls. A more detailed calibration and correlation study is underway; only general comparisons with limited experimental

data are included here. Test results available in the literature for four specimens with low shear span ratios are used for the comparisons.

Overview of tests – Two wall specimens tested by Hidalgo et al. (2002) (Specimens 10 and 16), and two specimens reported by Hirosawa (1975) (Specimens 74 and 152) are investigated here. These four wall tests were selected because they represent a variety of wall configurations, specimen sizes, and loading conditions. For each of the four selected test specimens, the amount of shear reinforcement provided was greater than or equal to the minimum specified in ACI 318-02 (2002), i.e., ρ_{min}=0.0025. General specimen information for the four wall tests is shown in Table 1. As shown in the table, all specimens had shear span ratios ($M/(Vl)$) between 0.35 and 1.0.

Specimens 10 and 16 had similar reinforcement configurations; the shear span ratio was the main varying parameter between the two specimens (0.69 and 0.35 for Specimens 10 and 16, respectively). Relatively low shear span ratios were achieved in the testing of these specimens via fixing the base of the walls and avoiding rotations at the top of the walls by applying the lateral load at specimen mid-height, which produces a linear bending moment distribution with moments equal in magnitude and opposite in direction applied at the wall ends. Both specimens were designed to fail in shear by providing a relatively large amount of longitudinal reinforcement at wall boundaries. Specimen 74, is the only specimen subjected to axial load, and is also the specimen with the largest shear span ratio ($M/(Vl)$ = 1.0). It was tested under a cantilever loading condition, with lateral load applied at the top of the wall. Another distinct property of the specimen is that the shear and flexural capacities (according to ACI 318-02) of the specimen are close, the shear capacity being slightly lower. Finally, specimen 152, having a barbell-shaped cross section, was tested as a short beam with a concentrated transverse load applied at mid-span. From symmetry, half of the specimen represents a short wall where half of the applied transverse load corresponds to an equivalent lateral load applied to the wall, yielding a shear span ratio of 0.56.

Model calibration – The analytical model was calibrated to represent the geometric properties of the wall specimens, using 8 model elements stacked along the height of each wall, where each model element consisted of 8 strips (panel elements) defined along the length of the wall. Two strips were defined for each boundary element of the specimens, whereas the remaining 4 were used to discretize the web. Similar to the case for the slender wall, a more refined discretization of the model did not change considerably the analytical responses obtained for the short walls, this issue is addressed in a subsequent section. Corresponding tributary areas for concrete and vertical reinforcement were assigned to each strip, whereas a constant horizontal reinforcement area was used for each strip. Similar to the case for the slender wall test, the constitutive material parameters were calibrated based on available experimental data reported on the mechanical properties of the materials used in the construction of the wall specimens.

Model correlation with test results – Figure 9 shows the correlation of experimental and analytical results for the lateral load-displacement response of each of the four wall specimens. Analytical results were not obtained for large lateral displacements values

within the post-peak (degrading) branch of analytical response, since the results in that range are subject to the so-called damage localization problem (i.e., analysis results for the degrading response are sensitive to the discretization of the model elements). Thus, degrading responses are not considered in the present study.

As observed in Fig. 9(a), a very good correlation is obtained between test results and results of the proposed coupled shear-flexure model for Specimen 74 ($M/(Vl)$=1.0). Since the design flexural and shear capacities of the specimen are close, to consider the possibility that the response of the specimen is governed by nonlinear flexural deformations (i.e., the specimen does not experience significant nonlinear shear deformations), Figure 9(a) also includes an analytical flexural response prediction (with shear deformations not considered) obtained using a fiber model. The same geometric discretization and material constitutive models used in the coupled model were adopted for the fiber model, with the distinction that the panel elements (strips) of the coupled model were replaced with uniaxial (fiber) elements, and the constitutive model used for concrete in compression did not incorporate the biaxial compression softening factor coefficient (β). Figure 9(a) illustrates that although the flexural (fiber) model provides a ballpark estimation of the wall lateral load capacity, (predicted lateral load capacities approximately 750 kN and 980 kN, respectively for the coupled and flexural models), the load-displacement response obtained by the flexural model is significantly different than the measured response and the coupled model response. After a lateral load of 450 kN, significant lateral stiffness degradation is observed in both the test results and results of the coupled model, but not in with the flexural model. This result demonstrates how the proposed model, which couples shear and flexural responses, is able to simulate observed responses with substantially greater accuracy than a flexural model, particularly for wall specimens where the nominal shear and flexural capacities are nearly equal.

The correlation between results of the coupled model and test results for Specimen 10 ($M/(Vl)$ = 0.69) is similar to that of Specimen 74 (Fig. 9(b)). The model provides a good prediction of the lateral load capacity and lateral stiffness of the wall specimen for most of the top displacement history, although the wall specimen reaches its peak lateral load capacity at a smaller top displacement than that predicted by the model. The sudden lateral load reductions observed in the model response are due to sequential cracking of concrete, whereas such behavior is not observed in test results. Refining the model discretization (increasing the number of strips used along the length of the wall) would invoke a more gradual and continuous shape for the analytical load-displacement response.

A relatively poor correlation is obtained between model and test results for the peak lateral load capacity of Specimen 152 ($M/(Vl)$ = 0.56), for which the model underestimates the peak lateral load capacity of the specimen by approximately 25% of the measured value (Fig. 9(c)). However, the analytical model provides a good prediction of the wall lateral stiffness at lower lateral load levels, and the general shape of the nonlinear response simulated by the model is reasonable.

However, the correlation for Specimen 16 ($M/(Vl)$ = 0.35) is far from being reasonable, where the analytical model under predicts the measured lateral load capacity of the wall by up to 50% for the entire loading history (Fig. 9(d)). Specimen 16 was subjected to the same loading conditions as Specimen 10 ($M/(Vl)$= 0.69), and also had a similar reinforcement configuration; the shear span ratio was the main differentiating parameter between the two specimens. Thus the difference between the accuracy in the predictions presented in Fig. 9(b) and Fig. 9(d) is associated directly with variation in shear span ratios of the two specimens.

Overall, the correlations indicate that the accuracy of the proposed model in predicting wall response is progressively impaired as the shear span ratio of the wall modeled is reduced. The best correlation is obtained for Specimen 74 ($M/(Vl)$ = 1.0), whereas results for Specimen 16 ($M/(Vl)$ = 0.69) were generally good. Results for Specimen 152 ($M/(Vl)$ = 0.56) showed a relatively poor but reasonable correlation, and the model was not successful in predicting the response of Specimen 16 ($M/(Vl)$ = 0.35). Therefore, it is apparent that the validity of the modeling approach and the model assumptions are violated as wall shear span ratios decrease. In a wall with a small shear span ratio, stresses and strains can follow significantly nonlinear distributions as opposed to the assumptions incorporated in the present model (uniform shear strain distribution and zero horizontal stress along wall length). Ongoing work focuses on improving the modeling methodology and assumptions, as well as conducting extensive correlation studies.

Sensitivity of analytical results to model discretization – A parametric study was conducted to investigate the sensitivity of the analytical results to the number of model elements stacked along wall height and the number of strips defined along wall length. The pre-peak region of the analytical load-displacement response was found to be insensitive to the selection of either the number of elements or the number of strips, provided that reasonable values are selected in order to adequately represent the overall wall geometry. Figure 10(a) shows a comparison of the lateral load-displacement responses predicted by stacking 8 model elements with a varying number of strips defined along the length of the wall specimen 74 (shear span ratio of 1.0). Figure 10(b) compares the results obtained using 8 strips along wall length, and varying the number of model elements stacked along wall height. The correlations presented in Figure 10 for specimen 74 is typical for all of the walls (including the slender wall specimen RW2) investigated herein.

Results shown in Figure 10(a) indicate that increasing the number of strips does not change significantly the predicted load-displacement response. However, increasing the number of strips invokes a more gradual and continuous shape for the response, with smaller magnitudes of sudden lateral load reductions due to sequential cracking of concrete (incursion into the post-peak region of the tensile stress-strain relation) within each strip. Figure 10(b) shows that the predicted lateral load capacity of the wall and the pre-peak region of the predicted load-displacement response are marginally sensitive to the number of elements stacked along the wall height. However, as shown in Figure 10(b), the variation in the wall capacity is not substantial for the walls investigated in this study.

Figure 10(b) also shows that the degrading region (and initiation of the degrading region) of the predicted load-displacement response is highly sensitive to the selection of the number of elements. This behavior is due to damage localization effects associated with the crushing of concrete in compression (incursion into the post-peak region of the compressive stress-strain relation). For the walls investigated, wall lateral load capacity is governed by the compressive strength of concrete (i.e., the failure mode is concrete crushing). Thus, the post-peak region of the stress-strain behavior of concrete in compression controls the degrading region of the analytical load-displacement response. The present model cannot reliably predict this strength degradation, without implementation of a proper damage localization parameter to calibrate the post-peak (descending) region of the compressive stress-strain behavior of concrete based on the size (height) of the elements used. This study focuses on predicting the pre-peak load-displacement response and the lateral load capacity of walls; modeling of damage localization and predicting degrading responses is not addressed.

Sensitivity of analytical results to the zero-resultant-horizontal-stress assumption – As discussed in a previous section, the validity of the modeling approach and the model assumptions are violated as wall shear span ratios decrease. In walls with relatively small shear span ratios (e.g., specimens 152 and 16), the distribution of stresses and strains can be significantly different than the assumptions incorporated in the present model (uniform shear strain distribution along wall length and zero resultant horizontal stress along wall length and height), impairing the correlation between model predictions and test results.

As part of ongoing studies to improve the formulation of the model for a better prediction of the response of walls with low shear span ratios, the sensitivity of the model results to variations in the zero resultant horizontal stress assumption was investigated. Prior studies by Cheng et al. (1993) revealed that, for walls with low aspect ratios (e.g., h/l = 0.5), the horizontal strains developed along the length of the wall are significantly reduced, especially in regions close to the top and bottom of the wall, partially due to the constraining effect of the pedestal (or beam) at the bottom and the beam at the top of the wall. Thus, for modeling, using an assumption of zero horizontal normal strain ($\varepsilon_x = 0$), especially in regions close to the top and bottom of the wall, may be more appropriate than assuming zero resultant horizontal stress ($\sigma_x = 0$) along the entire height of a wall with a low shear span ratio.

To investigate this idea, the formulation of the present model was modified to represent an extreme case of assuming zero horizontal strains ($\varepsilon_x = 0$) along the entire height and length of a wall, and the analysis was repeated for the wall specimens 152 ($M/(Vl)$=0.56) and 16 ($M/(Vl)$=0.35). The numerical methodology used to conduct the new analyses was simpler, since defining a zero value for the horizontal strain in each strip completes the definition of the strain field for each strip. Thus, the internal iteration scheme described in step 2 of the numerical methodology became redundant.

Figure 11 compares the results of the new analyses ($\varepsilon_x = 0$) with test results, as well as with analytical results obtained previously using a zero horizontal stress ($\sigma_x = 0$)

assumption. As shown in the figure, the analytical load - displacement responses obtained using the zero horizontal strain assumption yields much higher lateral stiffness and lateral load capacity for the walls, compared to results of the prior analyses obtained using the zero horizontal stress assumption. The experimentally obtained load-displacement responses fall in between these two analytical responses, which represent extreme cases associated with wall boundary conditions ($\sigma_x = 0$ is the static boundary condition at the sides of a wall, and $\varepsilon_x = 0$ is the kinematic boundary condition at the top and bottom of a wall with a rigid beams or pedestals at the top and bottom). Therefore, it is obvious that a more detailed description of the distribution of the horizontal normal strains and stresses is necessary for an accurate prediction of the response of these walls.

In this study, reasonable response predictions were obtained using the extreme zero horizontal stress assumption for a slender wall and for two short walls with shear span ratios of 1.0 and 0.69. Neither the zero horizontal stress nor the zero horizontal strain assumption worked well for walls with shear span ratios of 0.56 and 0.35. It must be noted that although specimen 16 ($M/(Vl) = 0.35$) had a relatively low shear span ratio, the aspect (height-to-length) ratio of this wall is twice its shear span ratio, since this wall was tested under loading conditions resulting in double curvature (with moments at wall ends equal in magnitude and opposite in direction). Furthermore, the transverse beams (pedestals) at the top and bottom of specimen 152 ($M/(Vl) = 0.56$) were relatively small (i.e., only twice as thick as the wall), possibly falling short of producing a pronounced "constraining effect" in the horizontal direction. Thus, the zero horizontal strain condition, as suggested by Cheng et al. (1993) for walls with low aspect ratios (i.e., $h/l = 0.5$) and with pedestals at top and bottom, may not have been a reasonable assumption in modeling the responses of these particular walls. The zero horizontal stress assumption also is inaccurate; however, better predictions were obtained and the results generally did not over-estimate the strength, stiffness, or ductility capacity. Further experimental and analytical studies are underway to characterize short RC wall behavior as well as to improve modeling assumptions.

SUMMARY AND CONCLUSIONS

An analytical model that couples wall flexural and shear responses is proposed. The model incorporates RC panel behavior described by a rotating-angle approach, similar to the RA-STM into the fiber-based Multiple Vertical Line Element Model (MVLEM). The simple envelop material models used for steel and concrete resulted in generally good predictions of panel responses under pure shear. Model results were compared with selected test results for a slender wall and four short wall specimens.

A reasonably good load-displacement prediction was obtained for the slender wall, considering that results of monotonic analysis were compared with cyclic test results. The model overestimated the flexural deformations and underestimated the shear deformations experienced by the wall specimen; however, the coupling of nonlinear shear and flexural responses was clearly represented.

Comparisons between model responses and test results for short walls showed that the accuracy of the proposed model in predicting wall responses is better for walls with

relatively higher shear span ratios. Comparing limited test results with preliminary model responses, the model was found to provide a good response prediction for walls with rather large shear span ratios (1.0 and 0.69). The ascending region of the analytical load-displacement responses was found to be insensitive to model discretization (i.e., number of model sub-elements used), provided that reasonable values are selected in order to adequately represent the overall wall geometry. Based on the correlations presented, it is recommended to use the material models implemented and the level of discretization used in this study to model the shear-flexural response of walls with relatively large shear span ratios.

Increasingly significant discrepancies were observed between the analytical and experimental results for walls with lower shear span ratios (0.56 and 0.35). Therefore, the modeling approach and assumptions need to be improved in order to obtain reliable response predictions for shorter walls. It has been observed that the model has the potential to provide improved response predictions for such short walls, upon modifying the model assumptions to a represent a reasonable distribution of horizontal stresses and strains in a wall. The model results are promising; ongoing work focuses on refinement of the analytical model and the adopted material constitutive relationships, incorporating cyclic response analyses, conducting extensive experimental calibration and correlation studies and implementing the model into a widely available analysis platform.

ACKNOWLEDGEMENTS

The work presented in this paper was supported in part by funds from the National Science Foundation under Grant CMS-9810012, as well as in part by the Earthquake Engineering Research Centers Program of the National Science Foundation under NSF Award Number EEC-9701568 through the Pacific Earthquake Engineering Research (PEER) Center, Project 533-2002. Prof. E. Taciroglu of UCLA is thanked for his assistance with the numerical implementation. Any opinions, findings, and conclusions or recommendations expressed in this material are those of the authors and do not necessarily reflect those of the sponsors or other individuals mentioned here.

REFERENCES

1. Belarbi, H. and Hsu, T.C.C., 1994, “Constitutive Laws of Concrete in Tension and Reinforcing Bars Stiffened by Concrete”, *ACI Structural Journal*, V. 91, No. 4, pp. 465-474.
2. Carreira, D.J. and Kuang-Han, C., 1985, “Stress-Strain Relationship for Plain Concrete in Compression”, *ACI Structural Journal*, V. 82, No. 6, pp. 797-804.
3. Cheng, F. Y., Mertz, G. E., Sheu, M. S., and Ger, J. F., 1993, “Computed versus Observed Inelastic Seismic Low-Rise RC Shear Walls”, *Journal of Structural Engineering*, ASCE, V. 119, No. 11, pp. 3255-3275.
4. Collins, M.P. and Porasz, A., 1989, “Shear Strength for High Strength Concrete”, *Bull.* No. *193* – Design Aspects of High Strength Concrete, Comite Euro-International du Beton (CEB), pp. 75-83.

5. Hidalgo, P.A., Ledezma, C.A., Jordan, R.M., 2002, "Seismic Behavior of Squat Reinforced Concrete Shear Walls", *Earthquake Spectra*, V. 18, No. 2, pp. 287-308.
6. Hirosawa, M., 1975, "Past Experimental Results on Reinforced Concrete Shear Walls and Analysis on Them", *Kenchiku Kenkyu Shiryo*, No. 6, Building Research Institute, Ministry of Construction, Japan.
7. Hsu, T.T.C. and Zhu R.R.H., 2002, "Softened Membrane Model for Reinforced Concrete Elements in Shear", ACI Structural Journal, V. 99, No. 4, pp. 460-469.
8. Mansour, M., Lee, J., and Hsu, T.T.C., 2001, "Cyclic Stress-Stress-Strain Curves of Concrete and Steel Bars in Membrane Elements", *Journal of Structural Engineering*, ASCE, V. 127, No. 12, pp. 1402-1411.
9. Massone, L.M. and Wallace, J.W., 2004, "Load – Deformation Responses of Slender Reinforced Concrete Walls", *ACI Structural Journal*, V. 101, No. 1, pp. 103-113.
10. Menegotto, M. and Pinto, E., 1973, "Method of Analysis for Cyclically Loaded Reinforced Concrete Plane Frames Including Changes in Geometry and Non-Elastic Behavior of Elements Under Combined Normal Force and Bending", *Proceedings*, IABSE Symposium, Lisbon, Portugal.
11. Orakcal, K., Wallace, J.W., and Conte, J.P., 2004, "Nonlinear Modeling and Analysis of Slender Reinforced Concrete Walls", *ACI Structural Journal*, V. 101, No. 5, pp. 688 - 699.
12. Orakcal, K. and Wallace, J.W., 2004, "Modeling of Slender Reinforced Concrete Walls", *Proceedings*, 13th World Conference on Earthquake Engineering, Vancouver, Canada.
13. Pang, X.D. and Hsu, T.T.C., 1995, "Behavior of Reinforced Concrete Membrane Elements in Shear", *ACI Structural Journal*, V. 92, No. 6, pp. 665-679.
14. Petrangeli, M., Pinto, P.E., and Ciampi, V., 1999, "Fiber Element for Cyclic Bending and Shear of RC Structures. I: Theory", *Journal of Engineering Mechanics*, ASCE, V. 125, No. 9, pp. 994-1001.
15. Popovics, S., 1973, "A Numerical Approach to the Complete Stress-Strain Curve of Concrete", *Cement and Concrete Research*, V. 3, No. 4, pp. 583-599.
16. Sayre, B., 2003, "Performance Evaluation of Steel Reinforced Shear Walls", *MS Thesis*, University of California, Los Angeles.
17. Thomsen IV, J.H. and Wallace, J.W., 2004, "Experimental Verification of Displacement-Based Design Procedures for Slender Reinforced Concrete Structural Walls", *Journal of Structural Engineering*; ASCE, Vol. 130, No. 4, pp. 618-630.
18. Vecchio, F.J. and Collins, M.P., 1982, "The Response of Reinforced Concrete to In-Plane Shear and Normal Stresses", *Publication* No. 82-03, Department of Civil Engineering, University of Toronto, Toronto, Canada.
19. Vecchio, F.J. and Collins, M.P., 1986, "The Modified Compressional-Field Theory for Reinforced Concrete Elements Subjected to Shear", *Journal of the American Concrete Insitute*, V. 83, No. 22, pp. 219-231.
20. Vecchio, F.J. and Collins, M.P., 1993, "Compression Response of Cracked Reinforced Concrete", *Journal of Structural Engineering*, ASCE, V. 119, No. 12, pp. 3590-3610.
21. Vulcano, A., Bertero, V.V., and Colotti, V., 1988, "Analytical Modeling of RC Structural Walls", *Proceedings*, 9th World Conference on Earthquake Engineering, V. 6, Tokyo-Kyoto, Japan, pp. 41-46.

22. Wee, T.H., Chin, M.S., and Mansur, M.A, 1996, "Stress-Strain Relationship of High-Strength Concrete in Compression", *Journal of Materials in Civil Engineering*, ASCE, V. 8, No. 2, pp. 70-76.
23. "Building Code Requirements for Structural Concrete – ACI 318-89", 1989, *American Concrete Institute*, Farmington Hills, Michigan.
24. "Building Code Requirements for Structural Concrete – ACI 318-02", 2002, *American Concrete Institute*, Farmington Hills, Michigan.
25. "OpenSees – Open System for Earthquake Engineering Simulation", *Pacific Earthquake Engineering Research Center*, University of California, Berkeley.

Reported by			Hidalgo et al. (2002)		Hirosawa (1975)	
Test no			10	16	74	152
lw	clear length	(cm)	130	170	170	208
hw	height	(cm)	180	120	170	152
tw	web thickness	(cm)	8	8	16	16
lb	boundary length	(cm)	-	-	-	32
tb	boundary thickness	(cm)	-	-	-	32
M/(Vl)	shear span ratio	-	0.69	0.35	1.00	0.56
ρh	web horizontal steel ratio	(%)	0.25	0.25	0.57	0.62
ρv	web vertical steel ratio	(%)	0.25	0.25	0.61	0.58
Ab	boundary vertical steel	(cm^2)	7.6	6	15.5	66.4
N	axial load	(kN)	0	0	533	0

Table 1 – Properties of the selected short wall specimens

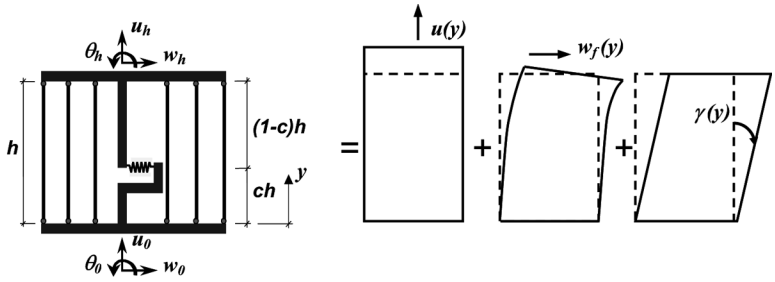

(a) MVLEM element (b) axial disp. (c) flexural disp. (d) shear disp.

Figure 1 – MVLEM element and incorporated displacement field components.

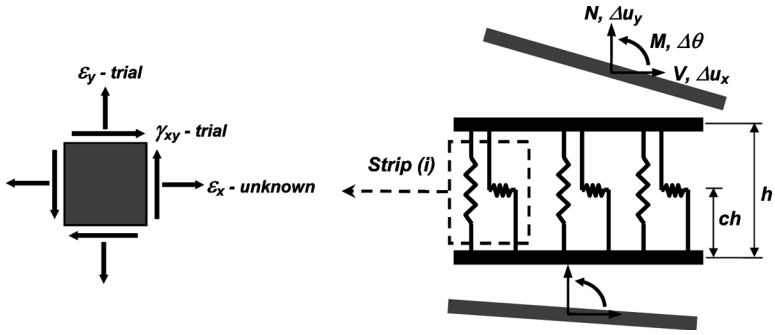

Figure 2 – Trial displacement state at section (*j*) of the coupled model element.

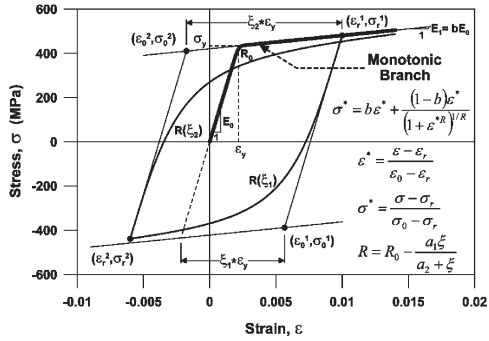

Figure 3 – Constitutive model for reinforcing steel.

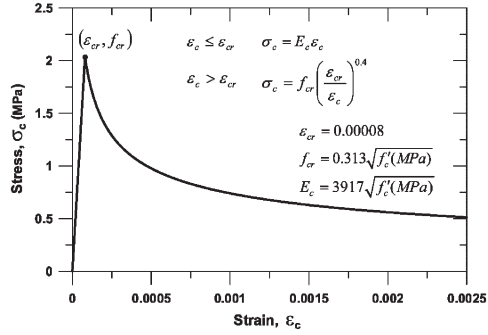

Figure 4 – Constitutive model for concrete in tension.

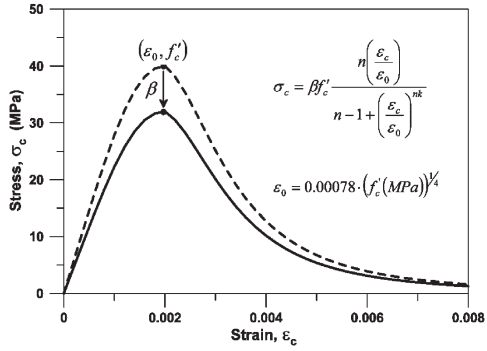

Figure 5 – Constitutive model for concrete in compression.

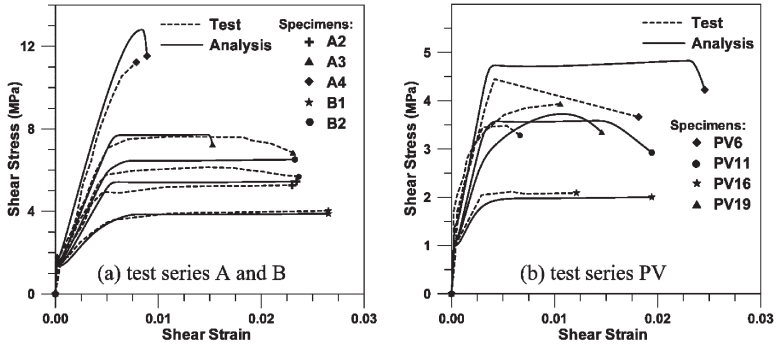

Figure 6 – Test results versus model element predictions for panel responses.

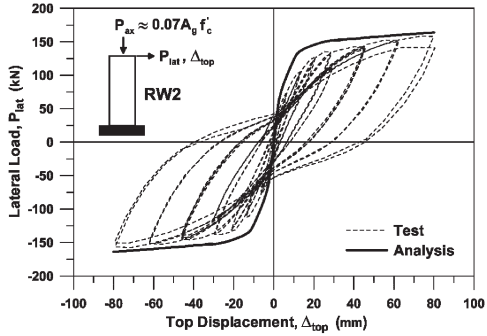

Figure 7 – Lateral load – top displacement response of Specimen RW2.

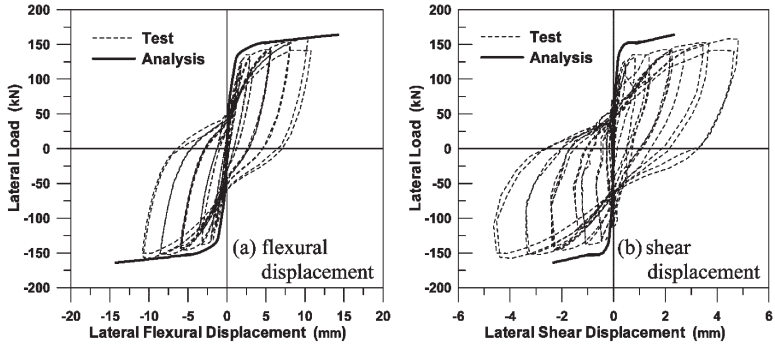

Figure 8 – Lateral load-displacement responses at first story level of Specimen RW2.

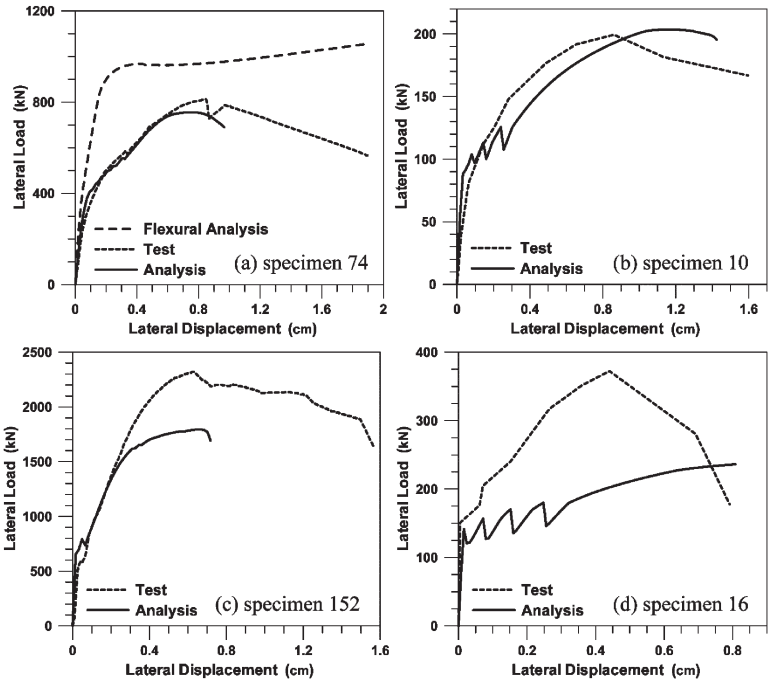

Figure 9 – Lateral load-displacement responses for the short wall specimens.

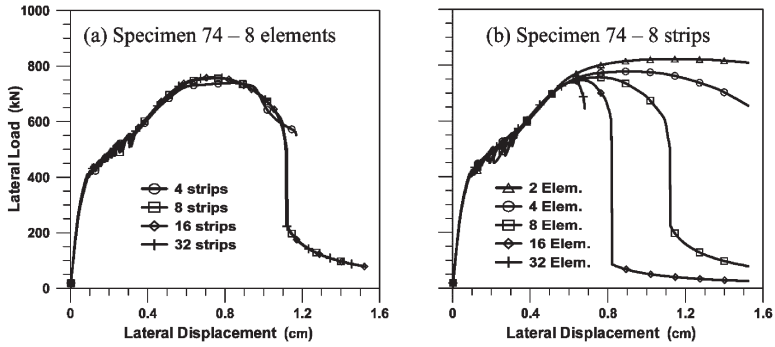

Figure 10 – Sensitivity of model results to number of strips and model elements.

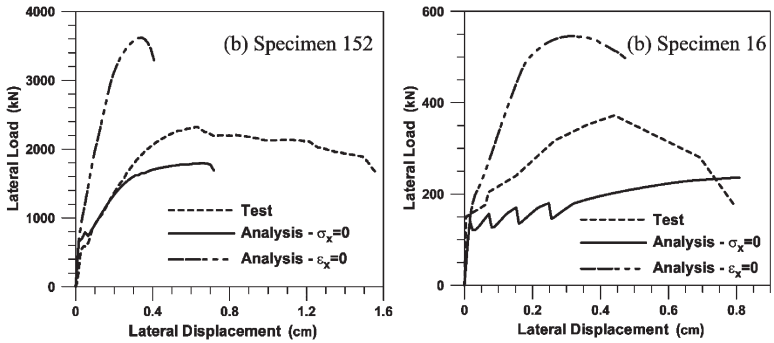

Figure 11 – Lateral load-displacement responses for short wall specimens 152 and 16 – zero horizontal stress and zero horizontal strain cases.